Exciton states in shallow ZnSe/(Zn,Mg)Se quantum wells: Interaction of confined and continuum electron and hole states

A. Pawlis,[1] T. Berstermann,[2] C. Brüggemann,[2] M. Bombeck,[2] D. Dunker,[2] D. R. Yakovlev,[2,3] N. A. Gippius,[4,5] K. Lischka,[1] and M. Bayer[2]

[1]*Department of Physics, University of Paderborn, D-33098 Paderborn, Germany*

[2]*Experimentelle Physik 2, Technische Universität Dortmund, D-44221 Dortmund, Germany*

[3]*A. F. Ioffe Physical-Technical Institute, Russian Academy of Sciences, R-194021 St. Petersburg, Russia*

[4]*LASMEA, Unité Mixte de Recherche 6602, Centre National de la Recherche Scientifique, Université Blaise Pascal, F-63177 Aubière, France*

[5]*A. M. Prokhorov General Physics Institute, Russian Academy of Sciences, R-119991 Moscow, Russia*

(Received 13 October 2010; revised manuscript received 16 December 2010; published 4 March 2011)

Exciton states have been studied experimentally in strained ZnSe/(Zn,Mg)Se quantum well structures with a Mg content of only 3.6% by means of magnetoreflectivity and ultrafast piezospectroscopy. The small intrinsic band gap difference and the built-in strain in barriers and quantum wells lead to a shallow confinement potential for heavy holes which is smaller than the Coulomb electron-hole interaction. An exciton state formed by a confined electron and heavy-hole continuum states is identified. The experimental findings are supported by numerical model calculations.

DOI: 10.1103/PhysRevB.83.115302 PACS number(s): 71.35.−y, 78.47.D−, 78.55.Et, 78.67.De

I. INTRODUCTION

The optical properties of semiconductor heterostructures are largely controlled by excitons, which are quasiparticles consisting of an electron and a hole bound by Coulomb interaction. Typically the exciton binding energies in III-V semiconductor heterostructures are considerably smaller than the confinement potentials given by the band-gap discontinuities, and therefore the Coulomb interaction is treated as a correction to the confinement energies of carriers. However, in quantum well (QW) structures with shallow confinement potentials, where the exciton binding energy becomes comparable or even larger than the confinement potentials, the Coulomb interaction has to be treated on the same level as the confinement potentials.[1,2] This is quite typical for heterostructures based on II-VI semiconductors, where the exciton binding energies are considerably larger than in III-V materials. For example, the exciton binding energy in bulk GaAs is 4.2 meV and in ZnSe is 20 meV, which may be further increased 2–3 times for quasi-two-dimensional excitons in QWs. There are several papers which report the experimental and theoretical study of excitons in ZnSe-based QWs (see Refs. 3–8, and references therein). All of them address the regime of relatively strong carrier confinement, while the excitonic states in shallow QWs based on II-VI heterostructures have not been examined in detail so far.

In addition to the confinement potentials determined by intrinsic band offsets, the strain in semiconductor heterostructures provides a further degree of freedom for tailoring the band structure.[9,10] Strain is induced by a lattice mismatch between the different layers of the QW and the barriers. In relatively thin heterostructures, the layers may be also strained due to a mismatch with the substrate lattice. Modern semiconductor fabrication techniques allow adjustment of the strain in a semiconductor heterostructure on a detailed level. Therefore strain might be exploited, for example, to improve the performance of electronic or optoelectronic devices.[11–13]

In this article, we report an experimental and theoretical study of the exciton states in a fully strained ZnSe/(Zn,Mg)Se QW with shallow confinement potentials for electrons and holes. In particular, the heavy-hole confinement potential is smaller than the exciton binding energy. The exciton resonances in reflectivity have been examined in magnetic fields and by modulation using ultrafast acoustics. These experiments reveal an exciton formed by the confined QW electron and heavy-hole continuum states in the barrier. These results are in good agreement with model calculations.

II. EXPERIMENT

The studied ZnSe/(Zn,Mg)Se heterostructure was grown by molecular-beam epitaxy (MBE) in a III-V/II-VI two-chamber machine. The (001)-oriented GaAs substrate with a thickness of 500 μm was overgrown by a 400-nm GaAs buffer layer on top of which the ZnSe/(Zn,Mg)Se heterostructure was grown at a temperature of 290 °C. First, a 20-nm-thick ZnSe buffer layer was deposited on the GaAs. Next, a 25-nm (Zn,Mg)Se layer was grown as bottom barrier layer, followed by the 10-nm ZnSe QW layer that was capped by the top barrier layer of 25-nm (Zn,Mg)Se. The structure is shown schematically in Fig. 1(a). The growth was performed in the phase-locked MBE mode and was monitored by *in situ* Reflection High Energy Electron Diffraction. An accuracy of a quarter of a monolayer (ML) in layer thickness was achieved in that way.

A reciprocal space map of the heterostructure, shown in Fig. 1(b), was measured close to the (224)-reflex with a high-resolution x-ray diffraction technique. Several clearly separated peaks, which are attributed to the GaAs substrate as well as the ZnSe and (Zn,Mg)Se layers, can be distinguished. All identified reflexes are aligned in the vertical direction, that is, they have the same q_x value. This confirms that the ZnSe and (Zn,Mg)Se layers are pseudomorphically, compressively strained on the GaAs substrate. For the ternary alloy

 ©2011 American Physical Society

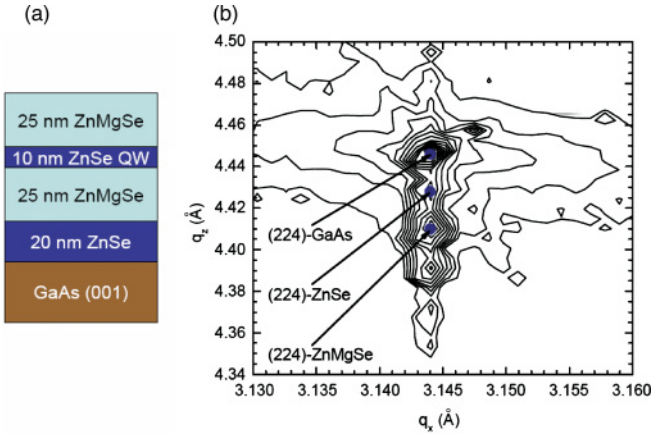

FIG. 1. (Color online) (a) Scheme of the ZnSe/(Zn,Mg)Se QW structure grown on GaAs substrate. (b) Reciprocal space map of the (224) reflex of the ZnSe/(Zn,Mg)Se heterostructure that is pseudomorphically and compressively strained on the GaAs substrate.

(Zn,Mg)Se barriers, a magnesium concentration of (3.6 ± 0.2)% was estimated from the reciprocal space map.

The low-magnesium mole fraction reduces alloy fluctuations in the ternary material and consequently reduces the inhomogeneous broadening of the excitonic transitions in both the barrier and in the QW. The band-gap difference between ZnSe and (Zn,Mg)Se with 3.6% magnesium amounts to 48.6 meV. This difference is split with a ratio 70/30 between the conduction and valence band.[7] The confinement potential of 36.8 meV for the conduction band electrons is sufficient to provide localization in a wide temperature range up to room temperature. The weaker hole confinements of 11.8 meV for heavy holes and 19.6 meV for light holes are comparable with the exciton binding energy of about 20 meV in bulk ZnSe. In this case, an exciton wave function cannot be attributed to a predominant hole level, but multiple hole levels may contribute.

For modeling the QW confinement potentials for electrons and holes, we used a finite barrier model approach including the compressive strain in the layers. The GaAs substrate enforces a biaxial strain of the layers in growth direction, which can be separated into an isotropic, hydrostatic pressure and an uniaxial strain component parallel to the z direction, which coincides with the structure growth axis. Hereby the renormalization of the band structure close to the Γ point of ZnSe and (Zn,Mg)Se is considered, using the theory of Pikus and Bir.[14] A detailed description of the formula sets applied especially for II-VI semiconductors can be found in Refs. 4,5 and 7.

In Table I, the main structural and electronic parameters of ZnSe and MgSe are summarized based on different literature sources.[4,5,7,15–18] Here m_e^*, m_{hh}^*, and m_{lh}^* are the effective masses of electron, heavy hole, and light hole, respectively; E_g is the unstrained band gap at $T = 5$ K; a_0 is the lattice constant of the unstrained material; c_{11} and c_{12} are the elastic stiffness constants; and a and b are the hydrostatic and tetragonal deformation potentials, respectively. All parameters of the (Zn,Mg)Se layers were obtained by linear interpolation between the binary material constants, to account for the magnesium concentration of 3.6% in our structure. Calculations including the strain-induced shifts of the bands and the strain-induced splitting of the heavy-hole and light-hole states in the ZnSe and (Zn,Mg)Se layers allow us to receive the band diagram of the studied QW, which is shown in Fig. 2.

TABLE I. Electronic and structural parameters of ZnSe and MgSe used for calculating the confinement potentials in the strained ZnSe/(Zn,Mg)Se heterostructure.

Parameter	ZnSe	MgSe	Refs.
m_e^*(units of m_0)	0.147	0.23	16,17
m_{hh}^*(units of m_0)	0.96	0.78	17
m_{lh}^*(units of m_0)	0.27	0.33	17
E_g (eV)	2.82	4.1	7
a_0 (nm)	0.566 86	0.5892	4,18
c_{11} (GPa)	82.6	63.1	4,18
c_{12} (GPa)	49.8	61.8	4,18
a (eV)	−4.25	−4.79	5,15
b (eV)	−1.2	−1.39	5,15

Reflectivity spectra were measured at normal incidence. The light of a halogen lamp reflected from the sample was dispersed by a 3 × 0.5 m triple spectrometer operated in the additive mode, providing a spectral resolution of ∼0.1 meV. The signal was detected by a charge-coupled device camera. For magnetoreflectivity experiments, the sample was immersed in helium gas at a temperature of $T = 5$ K, applying magnetic fields B up to 10 T, generated by a superconducting split-coil solenoid. The magnetic field was applied parallel to the structure growth axis and along the propagation direction of light (Faraday geometry). The reflected light was detected polarization resolved using a $\lambda/4$ plate and a Glan–Thompson prism in front of the spectrometer.

An ultrafast piezospectroscopy technique utilizing the injection of picosecond strain pulses into solids[19–22] was used to identify the exciton resonances with an in-depth resolution

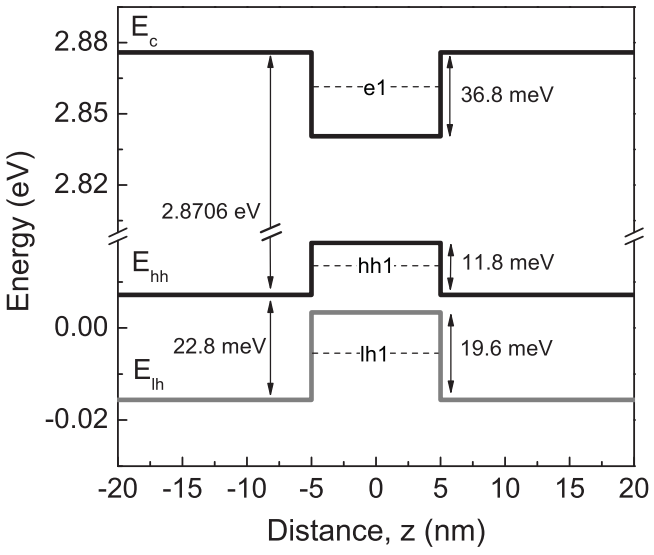

FIG. 2. Energy diagram of the confinement potentials for electrons, heavy holes, and light holes in the strained ZnSe/(Zn,Mg)Se QW with magnesium concentration of 3.6% vs the growth axis.

of their spatial location. For strain pulse injection, a 100-nm thin aluminum film was deposited on the backside of the GaAs substrate, which had been polished down to a thickness of 100 μm. The film was heated with a 150 fs laser pulse (wavelength 800 nm and repetition rate 100 kHz) using typical excitation densities P on the film of $\sim$1 mJ/cm^2. Due to rapid thermal expansion of the metal film, a picosecond bipolar uniaxial strain pulse was injected into the GaAs substrate. This pulse propagates with the speed of longitudinal sound so that it reaches the II-VI heterostructure $\sim$20 ns after the excitation process.

We measured the changes in the reflectivity spectra induced by the picosecond strain pulses with a time-resolved pump-probe technique.[21] To access the reflectivity, white-light pulses were generated by sending a part of the source laser pulse through a sapphire plate. The white light was focused on the front side of the sample exactly opposite to the strain pulse excitation spot (see the inset of Fig. 5). The white-light pulses were delayed using a mechanical delay line such that they hit the QW when the strain pulse arrived. The time delay could be varied with a step of 300 fs. This enabled time-resolved scanning of the influence of the strain pulse on the reflectivity spectra. The reflectivity spectra were detected with a 0.5-m spectrometer with a spectral resolution of $\sim$0.3 meV. The measurements were carried out at $T = 5$ K, with the sample immersed in helium gas.

III. REFLECTIVITY AND MAGNETOREFLECTIVITY

A reflectivity spectrum of the ZnSe/(Zn,Mg)Se QW structure is shown in Fig. 3(a). Four pronounced resonances appear in the spectrum at energies 2.8107, 2.8272, 2.8334, and 2.8506 eV. Two of them, positioned at lower energies, have a full width at half maximum of 1.2 meV. The two other resonances at higher energies are broader, having widths of 2.2 meV.

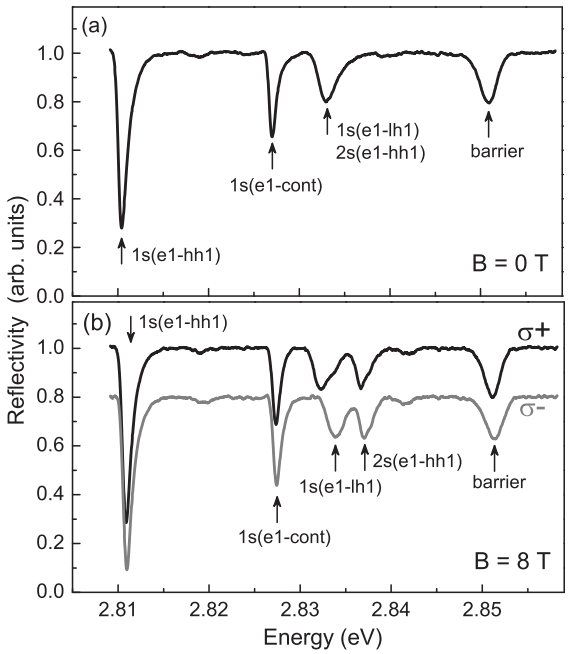

FIG. 3. Reflectivity spectra of the ZnSe/(Zn,Mg)Se QW sample measured at $T = 5$ K. (a) Spectrum without magnetic field. (b) Spectra for σ^+ and σ^- polarized detection at a magnetic field $B = 8$ T in Faraday geometry. The spectrum in the σ^- polarization is shifted vertically for clarity. The resonance labels are explained in the text.

The energetically highest lying resonance at 2.8506 eV is located about 20 meV below the expected band gap of (Zn,Mg)Se for a magnesium concentration of 3.6%. Note that the exciton binding energy in ZnSe is 20 meV,[23] and therefore this resonance can be attributed to the exciton in the (Zn,Mg)Se barrier. We obtained further evidence for this assignment from the ultrafast piezospectroscopy experiments described in Sec. IV.

The resonance at 2.8107 eV has the largest oscillator strength and is shifted by about 10 meV to higher energies relative to the exciton energy in ZnSe.[23] This shift is contributed by the quantum confinement energy of electrons and holes in the QW and by the increase of the binding energy of the quasi-two-dimensional exciton.[7,8] Consequently, the resonance at 2.8107 eV can be attributed to the 1s state of the QW exciton consisting mainly of the confined electron ground state in the conduction band ($e1$) and the confined heavy-hole ground state in the valence band ($hh1$) (see Fig. 2). We label this resonance accordingly with 1s($e1$-$hh1$). The origins of the two other resonances at 2.8272 and 2.8334 eV are not so obvious. They may be related to the 1s exciton involving the light hole or to the 2s($e1$-$hh1$) exciton. As we will show below, also, an excitonic state, which is particularly relevant in shallow QWs due to its closeness to the ground state exciton, can be formed, which is composed of the confined $e1$ electron and heavy-hole states from the above-barrier continuum.

Application of a strong external magnetic field and polarization-resolved detection of the optical spectra are powerful techniques for investigating exciton resonances in QW structures.[8,24] An example of circularly polarized reflectivity spectra is shown in Fig. 3(b) for a magnetic field of $B = 8$ T. Three resonances at 2.8107, 2.8272, and 2.8506 eV show very weak diamagnetic shifts and Zeeman splittings, while the resonance at 2.8334 eV is clearly split by 1.6 meV and a new resonance appears in the spectrum at 2.837 eV.

Figure 4(a) shows the magnetic field dependence of the resonance energies. Open and closed symbols correspond to σ^+ and σ^- polarization, respectively. The three resonances labeled 1s($e1$-$hh1$), 1s($e1$-cont), and "barrier" show weak diamagnetic shifts with coefficients of 6–7 μeV/T^2, which is an indicator of the 1s character of these states. No significant Zeeman splitting is found for them [see also Fig. 4(b)], which indicates that the corresponding values of the exciton g factors do not exceed 0.2. Such a small exciton g factor is typical for the 1s($e1$-$hh1$) state in ZnSe based QWs[8,24] and is related to the fact that the electron (g_e) and heavy-hole (g_{hh}) g factors are close to each other so that they almost compensate each other in the exciton Zeeman splitting determined by the g factor $g_X = g_{hh} - g_e$.[8,25] The electron g factor in ZnSe is $g_e = +1.12$ (see Ref. 26, and references therein) and has only a weak dependence on QW width in ZnSe-based structures.[8] According to the definitions used in Refs. 8 and 25, the exciton g factor is positive when the lowest energy Zeeman component is σ^+ polarized, as is the case for the studied structures. Therefore, the hole g factors for the 2.8107, 2.8272, and

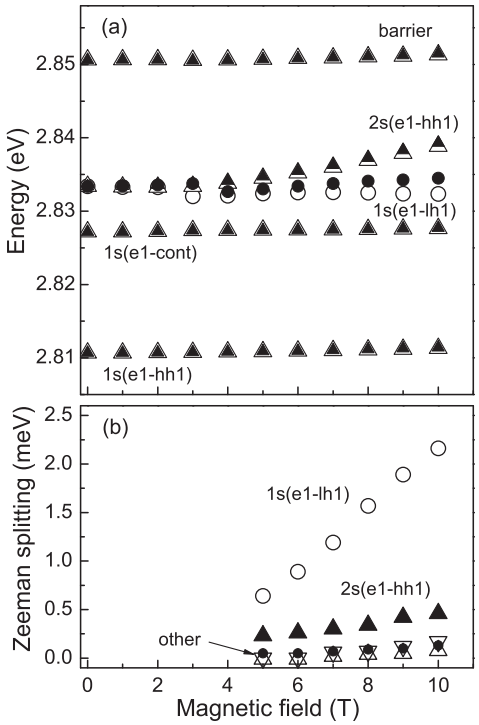

FIG. 4. Magnetic field dependence of the exciton resonance energies in the ZnSe/(Zn,Mg)Se QW. (a) Triangles and circles indicate heavy-hole and light-hole exciton transitions, respectively. Full symbols denote σ^+ and open symbols refer to σ^- polarized detection. (b) Zeeman splitting for the light-hole state (open circles) and the 2s heavy-hole state (closed triangles). Remaining resonances are labeled "other."

2.8506 eV resonances are positive, and their values slightly exceed the one of the electron, that is, $g_{hh} > +1.12$.

The resonance at 2.8334 eV has a large Zeeman splitting corresponding to $g_X = +3.72$. Based on the splitting at $B = 10$ T, one obtains an effective hole g factor of $+4.84$. The Zeeman splitting is a nonlinear function of the magnetic field, which shows that the mixing of light-hole and heavy-hole states is changed with increasing magnetic field [see Fig. 4(b)]. The energy separation of this resonance of 22.7 meV from the 1s(e1-hh1) exciton, in combination with its large g factor, allows us to assign it to the exciton involving the light-hole ground state, labeled accordingly 1s(e1-lh1) exciton.

The new line, which emerges from the 1s(e1-lh1) exciton line at magnetic fields above 3 T [see Figs. 3(b) and 4(a)], shows a very strong diamagnetic shift with a coefficient of 62 μeV/T^2. This allows us to assign it to the 2s state of the (e1-hh1) exciton. The energy splitting from the 1s(e1-hh1) state can be estimated to be 22.1 meV at zero magnetic field by extrapolating the resonance energy shift to $B = 0$ (2.8328 eV). This value corresponds to the binding energy of the quasi-two-dimensional exciton of about 26 meV, which is in good agreement with results of model calculations.[8] The Zeeman splitting of the 2s(e1-hh1) state, shown by closed triangles in Fig. 4(b), is a linear function of the magnetic field, giving $g_X = +0.79$ and $g_{hh} = +1.91$. Note that the exciton g factors of the 1s and 2s exciton states involving the very same confined carriers are not equal to each other. We suggest that this difference has the same origin as the recently reported energy dependence of the exciton g factor in thick layers of GaAs, CdTe, and ZnSe,[27–29] which was explained by the motion-induced mixing of the 1s ground state with excited p states.

To summarize this section, four of the five resonances in the magnetoreflectivity spectra could be identified. However, the strong and sharp resonance at 2.8272 eV, prospectively labeled as 1s(e1-cont), is not convincingly identified so far. The negligible diamagnetic shift and the small Zeeman splitting favor a 1s character involving heavy-hole valence band states.

IV. PIEZOSPECTROSCOPY WITH PICOSECOND STRAIN PULSES

Insight into the spectral origin of the observed exciton states can be obtained through ultrafast acoustic experiments. Figure 5 shows a spectral-temporal contour plot of the reflectivity spectra when a strain pulse ($P = 4$ mJ/cm^2) propagates through the ZnSe/(Zn,Mg)Se heterostructure. The time delay $t = 0$ is chosen such that it marks the first indication of a response of the barrier exciton resonance energy to the applied strain pulse. The strain pulse first shifts all resonances to higher energies due to compression of the lattice and thereafter induces lower energy shifts due to the tensile part of the strain pulse.[20] The lower energy shift is affected by superposition of the compressive forefront of the strain pulse, which was reflected at the top surface of the heterostructure

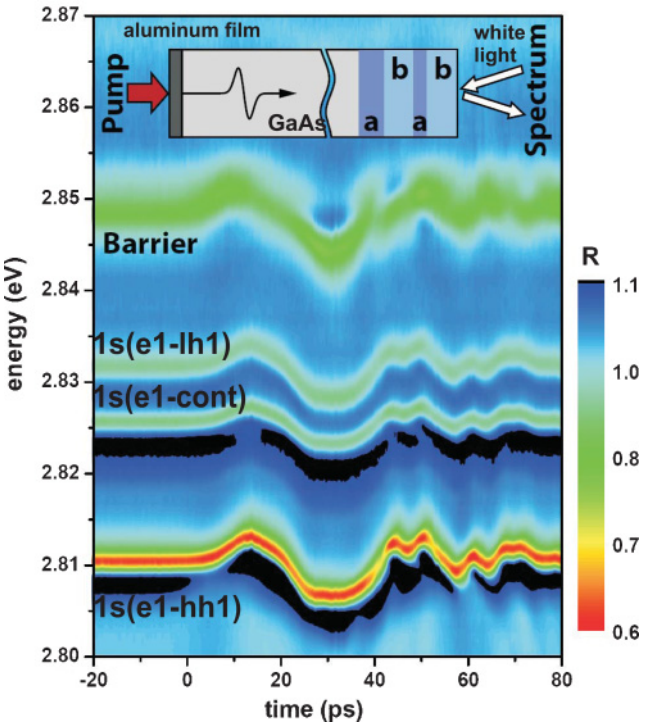

FIG. 5. (Color online) Spectral-temporal contour plot of the reflectivity of the ZnSe/(Zn,Mg)Se QW reflecting the impact of a strain pulse excited using an energy density $P = 4$ mJ/cm^2. $T = 5$ K. The inset shows the experimental geometry, where layers (a) are ZnSe and (b) (Zn,Mg)Se.

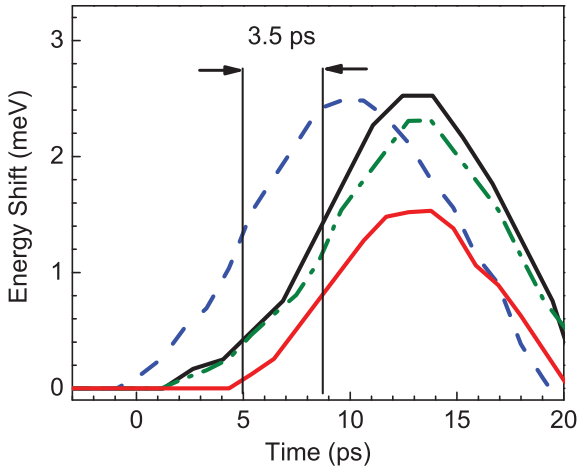

FIG. 6. (Color online) Time evolution of the energy shifts of the four strongest resonances relative to their equilibrium energy [blue dashed line, barrier; black solid line, 1s(e1-hh1); green dash-dotted line, 2s(e1-hh1); red solid line, 1s(e1-cont)]. $P = 4$ mJ/cm^2. The shift of the barrier exciton occurs 3.5 ps before the shifts of the other resonances set in.

with a phase shift of π and of the trailing tensile edge of the incoming pulse.[20]

The three lowest energy resonances show very similar time evolutions, differing mainly by the amplitude of the strain-induced energy shift. These shifts are comparable for 1s(e1-hh1) and 1s(e1-lh1), but in comparison, the one of the 1s(e1-cont) resonance is about 40% smaller (see also Fig. 6 for details).

One also sees in Fig. 5 that, as expected, the time-resolved signal of the barrier exciton differs from the behavior of the 1s(e1-hh1) and 1s(e1-lh1) QW exciton resonances: (a) the barrier resonance reacts to the strain pulse modulation at earlier times and (b) the shape of the modulated signal is different. The latter is clearly seen for the low-energy shift, which is not influenced by the superposition of incoming and surface-reflected strain pulse components. Both observations reflect that the barrier and QW signals are formed at different depths of the ZnSe/(Zn,Mg)Se heterostructure. Note that the spatial resolution of the used technique is about ∼10 nm, being limited by the spatial extensions of the strain pulse as well as of the heterostructure layers. These results indicate that piezospectroscopy may be used for analyzing the layer sequence in heterostructures with a resolution of about 10 nm.

Figure 6 shows the dynamics of the resonance shifts for time delays shortly after $t = 0$, focusing on the initial high-energy shifts. A clear temporal shift of the barrier signal by 3.5 ps to earlier times compared to the other signals is seen. The left vertical line indicates the delay time t when the barrier exciton shift reaches half of its maximum value. The right vertical line indicates the same for the three other resonances. From the sound velocity for ZnSe $v_{\mathrm{ZnSe}} = 4 \times 10^3$ m/s,[23] the 3.5-ps separation corresponds to a distance of 14 nm, which is in reasonable agreement with the distance of 17.5 nm from the center of the (Zn,Mg)Se barrier to the ZnSe QW center.

We focus now again on the 1s(e1-cont) exciton resonance and discuss two experimental findings for it: (a) The response of this resonance to the applied strain pulse is synchronous to

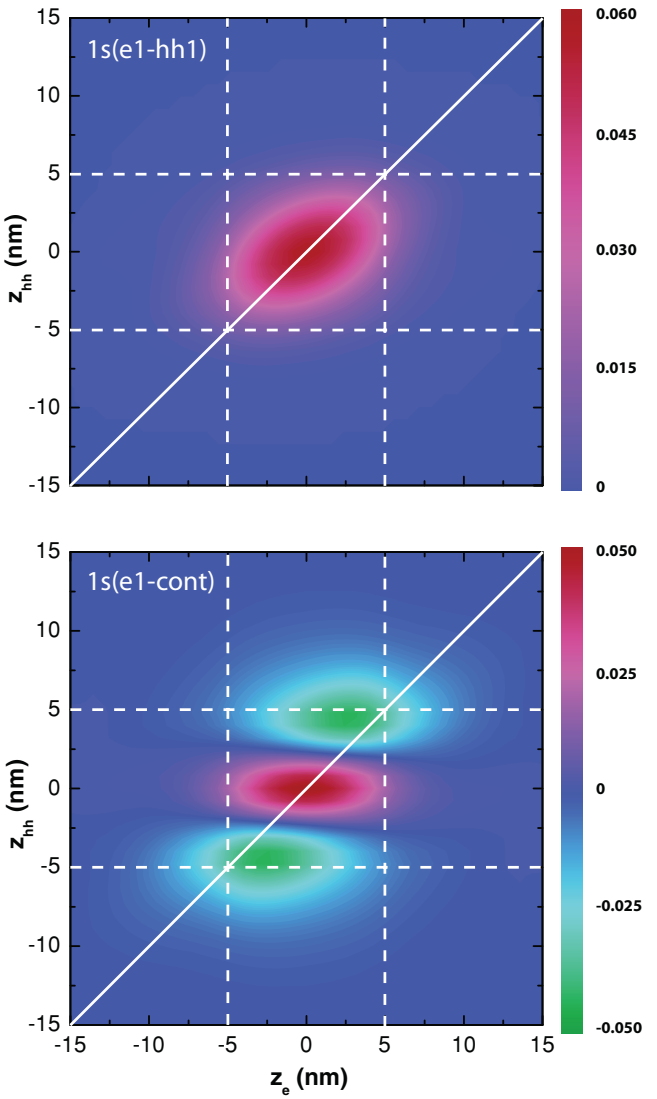

FIG. 7. (Color online) Exciton wave function of the two lowest e-hh exciton states plotted as a function of the z coordinates of electron and hole for equal in-plain coordinates (i.e., $\rho = 0$, $\boldsymbol{\rho} = \boldsymbol{\rho}_e - \boldsymbol{\rho}_h$). Dashed lines show the positions of the QW interfaces.

the responses of the 1s(e1-hh1) and the 1s(e1-lh1) exciton and (b) the maximum spectral shift during the first compressive part (at $t = 13$ ps) is only 65% of that of the 1s(e1-hh1) exciton.

The first result clearly indicates that the spatial origin and the extension of the 1s(e1-cont) state along the heterostructure growth direction is comparable to those of the QW excitons. The calculations discussed below confirm that an exciton composed of a QW electron and delocalized hole continuum states can become localized so that it is extended only over the QW (see Fig. 7). This requires a superposition of states such that they interfere constructively in the vicinity of the QW electron; well away from it, destructive interference occurs.

The obtained energy shift of the 1s(e1-cont) exciton is contributed by the shifts due to the deformation potential interaction in the conduction band and the valence band. While in the conduction band, the same shifts for the 1s(e1-cont) and 1s(e1-hh1) are expected, the behavior might be substantially

different for the complex valence band state. Most likely the components in this superposition state are affected differently by the strain pulse so that most probably the shift is smaller than for a confined hole state with well-defined spatial character.

Still this state with a $1s$ character, due to its small diamagnetic shift, may be composed of either a localized electronic state and delocalized continuum hole states or vice versa. The latter option is, however, very unlikely due to the considerably stronger confinement of the electrons compared to the holes.

V. MODEL CALCULATIONS

We will follow here the approach developed in Refs. 8 and 30. The main goal of the calculations is to clarify the origin of the exciton resonance with strong oscillator strength observed at 2.8272 eV and to corroborate our tentative assignment of this resonance to an exciton state composed of the $e1$ electron and heavy-hole continuum states. The hole is localized in the QW vicinity by the attractive Coulomb potential of the confined electron.

For shallow QWs, the exciton states are not "pure" states contributed by an electron and a hole from well-defined quantum-confined levels only, but many states contribute with various strengths. In this section, we will describe the calculation of exciton levels in QWs with band offsets comparable to the exciton Rydberg. The calculations of exciton states in this article were done in parabolic approximation; that is, the admixture of light-hole states and the effects of nonparabolicity were neglected. Within these approximations, the QW electron-hole (e-h) Hamiltonian has the form

$$H = H_{ez} + H_{hz} + H_{2D} + U_{eh} \equiv H_0 + U_{eh}. \tag{1}$$

Here

$$H_{jz} = -\frac{\hbar^2}{2m_j^z}\frac{\partial^2}{\partial z_j^2} + V_j(z_j), \qquad j = e,h. \tag{2}$$

$V_j = \Delta E_C(\Delta E_V)$ are the band-offset potentials in the conduction (valence) band and m_e^z and m_h^z are the electron and heavy-hole effective masses along growth direction, respectively. We will not account for the weak anisotropy of the electron effective mass in QW structures; that is, we take $m_e^z = m_e^{xy} = m_e$.

The Hamiltonian H_{2D} describes the two-dimensional (2D) motion of a free electron-hole pair in the QW plane:

$$H_{2D} = -\frac{\hbar^2}{2m_e}\nabla^2_{\boldsymbol{\rho}_e} - \frac{\hbar^2}{2m_h^{xy}}\nabla^2_{\boldsymbol{\rho}_h}, \tag{3}$$

where $\boldsymbol{\rho}_{e(h)}$ are the in-plane coordinates of electron (hole), $\boldsymbol{\rho} = \boldsymbol{\rho}_e - \boldsymbol{\rho}_h = (x,y)$. We neglect here the mass difference between the well and the barrier layers, which is justified by the very small content of Mg in the barrier layers.

The last term U_{eh} in Eq. (1),

$$U_{eh}(\rho, z_e, z_h) = -\frac{e^2}{\varepsilon}\left[\frac{1}{\sqrt{\rho^2 + (z_e - z_h)^2}}\right], \tag{4}$$

is the Coulomb interaction between electron and hole, where e is the electron charge and ε is the dielectric constant.

The quantization of the electron and hole states along the structure growth axis (z axis) provides the proper basis states. However, the small value of the band offset does not allow us to limit the expansion to confined states of electrons and holes only. In fact, we have to expand the exciton wave function in a series:

$$\psi(\rho, z_e, z_h) = \sum A_{i,j,n}\xi_i(z_e)\zeta_j(z_h)\psi_n(\rho), \tag{5}$$

where $\xi_i(z_e)$, $\zeta_j(z_h)$ are the sets of solutions of the 1D Schrödinger equation for electron and hole along the z direction [Eq. (2)] that contain not only confined states but also barrier continuum states. In the calculations we considered a finite slab containing the QW in the center, and we verified that the results do not depend significantly on the width of the calculation slab, provided its width exceeds 60 nm for a 10-nm-thick QW.

The radial basis $\psi_n(\rho)$ can be taken from the solution of the radial problem for the e-h pair [Eq. (3)], coupled by the effective potential $U_{\text{eff}}(\rho)$. For the s exciton (with angular momentum projection of the relative e-h motion $l_z = 0$ and total exciton momentum $\boldsymbol{K} = 0$), this equation reads as

$$\left[-\frac{\hbar^2}{2\mu}\frac{1}{\rho}\partial_\rho\rho\partial_\rho + U_{\text{eff}}(\rho)\right]\psi_n(\rho) = E_n^X\psi_n(\rho), \tag{6}$$

where $\mu = (1/m_e + 1/m_h^{xy})$ is the reduced exciton mass.

Equation (5) represents the basis set for calculating the exciton binding energy by diagonalization of the respective matrix. In case of strong confinement (i.e., when the Coulomb interaction is significantly smaller than the separation between quantum confined states), one can neglect the excited single-particle states, and the exciton problem reduces to a 1D radial equation with the Coulomb potential weighted over the ground states of electron and hole [see Eq. (9)] with $i,j,i',j' = 1$. However, in the case of a shallow (or wide) QW, where the energy separation between quantum confined levels is relatively small, such a reduction of the basis along the growth direction is not possible.

The matrix elements of the Hamiltonian [Eq. (1)] in the basis of Eq. (5) can be written in the following form:

$$H^{ijn}_{i'j'n'} = \left(E_i^e + E_j^h + E_n^X\right)\delta_{ii'}\delta_{jj'}\delta_{nn'} + \langle ijn|U_{eh}|i'j'n'\rangle - \delta_{ii'}\delta_{jj'}\langle n|U_{\text{eff}}|n'\rangle. \tag{7}$$

Here E_i^e and E_j^h are the quantum confined energies of electron and hole from Eq. (2) and E_n^X are the eigenvalues of the radial exciton from Eq. (6) with the effective interaction potential $U_{\text{eff}}(\rho)$ that can be taken as, for example, a Coulomb potential averaged over the electron and hole ground states $U_{11}^{11}(\rho)$ [see Eq. (9)]. The matrix element of the Coulomb potential can be calculated by

$$\langle ijn|U_{eh}|i'j'n'\rangle = \int 2\pi\rho d\rho \;\; U_{ij}^{i'j'}(\rho)\psi_n(\rho)\psi_{n'}(\rho), \tag{8}$$

where

$$U_{ij}^{i'j'}(\rho) = \int dz_e \int dz_h U_{eh}(\rho, z_e, z_h)\xi_i(z_e)\xi_{i'}(z_e)\zeta_j(z_h)\zeta_{j'}(z_h). \tag{9}$$

The effective interaction potential $U_{\text{eff}}(\rho)$ added to the radial part of the free e-h Hamiltonian in Eq. (6) should be

compensated by subtraction from U_{eh}, which, after integration over z_e and z_h, results in the last term in Eq. (7).

The diagonalization of the Hamiltonian [Eq. (7)] provides eigenvalues and eigenfunctions of the exciton states. The dimension of the basis depends on the ratio of quantization energy and Coulomb interaction. The wider the QW and, consequently, the smaller the vertical quantization is, the larger should be the number of z functions taken into account. In our calculation we have used 15 electron states, 30 hole states, and 10 radial basis functions. A further increase of the state numbers results in less than 0.2 meV change of the exciton energies.

VI. COMPARISON WITH EXPERIMENT AND DISCUSSION

The calculations were performed using the parameters for ZnSe-based QWs from Ref. 8: the dielectric constant $\varepsilon = 9.0$. We took the valence band offset value of 30% based on a detailed study of ZnSe/(Zn,Mg)Se QWs with higher Mg concentrations.[7] The carrier effective masses are given in Table I. The exciton in-plane reduced effective mass μ for ZnSe-based QWs typically is in the range from 0.10 to 0.12. We took it as free parameter and obtained best agreement with the $1s(e1\text{-}hh1)$ exciton energy in experiment for $\mu = 0.12$.

The calculated energies are compared to the experimental data in Table II, from which reasonable agreement is seen. The energies of the exciton resonances coincide within 1–2 meV. This is a reasonable agreement, taking into account the approximations discussed above, in particular, the parabolic approximation and the neglecting of the coupling between heavy-hole and light-hole states. Also the experimental energy difference between the $1s$ and the $2s$ state of the $(e1\text{-}hh1)$ exciton of 22.1 meV agrees well with the calculated value of 19.9 meV.

The central point of the calculations is the energy of the exciton state, which involves the $e1$ confined electron and the heavy-hole continuum. The localization potential for the heavy hole in the studied QWs is largely given by the Coulomb attraction of the confined electron. The predicted energy of $1s(e1\text{-cont})$ transition of 2.8269 eV is in good accord with the energy of 2.8272 eV measured in the reflectivity spectrum (see Table II).

TABLE II. Comparison of experimental exciton resonance energies and the ones calculated using a reduced exciton mass 0.12 and valence band offset of 30%.

	Experiment (eV)	Model (eV)
	Transitions	
$1s(e1\text{-}hh1)$	2.8107	2.8091
$1s(e1\text{-cont})$	2.8272	2.8269
$2s(e1\text{-}hh1)$	2.8328[a]	2.8290
$1s(e1\text{-}lh1)$	2.8334	2.8299
	Offsets	
$1s(e1\text{-}hh1)$ to $2s(e1\text{-}hh1)$	22.1	19.9
$1s(e1\text{-}hh1)$ to $1s(e1\text{-cont})$	16.5	17.7
$1s(e1\text{-}hh1)$ to $1s(e1\text{-}lh1)$	22.7	20.8

[a]Obtained by extrapolation of the diamagnetic shift of the $2s$ state to $B = 0$ T.

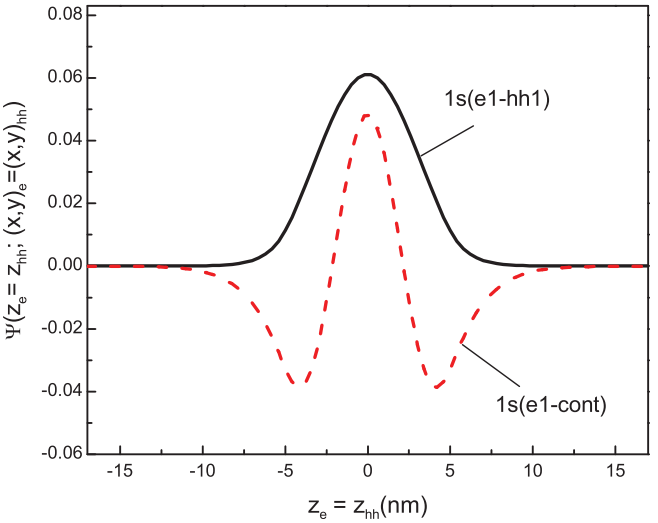

FIG. 8. Exciton wave function for coinciding coordinates of electron and hole. The oscillator strength of the exciton transition is given by the square of the integral of this plot.

Plots of the exciton wave functions for electron and hole located at the same position normal to the growth direction [i.e., with identical in-plane coordinates, $\Psi(z_e, z_{hh}, \rho = 0)$] as functions of the coordinates z_e, z_{hh} are given in Fig. 7 for the two lowest exciton states. In Fig. 8 we plot the Ψ values along the diagonal of Fig. 7, corresponding to $z_e = z_{hh}$. The square of the integral of this function over $z_{e(hh)}$ gives the exciton oscillator strength. One can see from these figures that the exciton wave function for the $1s(e1\text{-}hh1)$ state formed from confined carriers has a Gauss-like shape with one maximum. For the $1s(e1\text{-cont})$ exciton involving a high amount of admixed hole continuum states, the corresponding wave function has three maxima as a result of interference of ground and excited states of both electron and hole. The calculated wave functions confirm the experimentally measured accordance of their spatial extension.

We also want to point out that within the current approach, the hh and lh states have been calculated independently from each other. The main qualitative result—formation of the $1s(e1\text{-cont})$ state—will be valid in more detailed calculations. The energy of the $1s(e1\text{-cont})$ state, however, is much more sensitive to the number of hole states taken into account compared to the $1s(e1\text{-}hh1)$ and $1s(e1\text{-}lh1)$ states. Its energy is shifted down relative to the $2s(e1\text{-}hh1)$ state by increasing the number of hole states up to 30 and then remains unchanged within 0.2-meV accuracy. Most likely, accounting for the admixture of lh states will further increase the splitting between the $1s(e1\text{-cont})$ and $2s(e1\text{-}hh1)$ states, which would help to approach the experimentally observed energy.

We have examined the influence of the hole band offset on the transition energies by running model calculations for various offsets. The offset variation appeared to affect differently $1s(e1\text{-}hh1)$, $2s(e1\text{-}hh1)$ and $1s(e1\text{-cont})$ transitions. The $1s(e1\text{-}hh1)$ and $2s(e1\text{-}hh1)$ states practically do not depend on the hole offset varied in the range 0%–35%. To the contrary,

the $1s(e1\text{-cont})$ energy is 7 meV smaller than the $2s(e1\text{-}hh1)$ energy in case of zero offset. It shows a linear increase with growing offset and coincides with the $2s(e1\text{-}hh1)$ energy for a 30% offset. The experimentally observed splitting between $1s(e1\text{-cont})$ and $2s(e1\text{-}hh1)$ of 5.6 meV can be obtained in the calculations for 7% hole band offset.

In conclusion, the exciton states in shallow ZnSe/(Zn,Mg)Se QWs have been examined by magnetoreflectivity and ultrafast piezospectroscopy. In addition to the known $1s$ and $2s$ exciton states composed from quantum confined carriers in their ground states ($e1$, $hh1$, and $lh1$), a strong excitonic resonance, which involves the confined $e1$ electron and hole states from the above-barrier continuum, has been identified experimentally and modeled theoretically. Such an exciton is particularly relevant for shallow QWs, when it is located close to the ground-state excitons. In deep QWs, such states are also formed but are typically located on top of multiple exciton continua, with which they may become mixed. Therefore they are much harder to identify than in the case discussed here. Moreover, for deeper wells, the roles of nonparabolicity and mixing of heavy-hole and light-hole states become more important and should be properly accounted for by calculations.

ACKNOWLEDGMENTS

This work was supported by the Deutsche Forschungsgemeinschaft (Grant No. GRK-1464 and No. BA1549/14-1, respectively) and by the EU Seventh Framework Program (Grant No. 237252, Spin-optronics).

[1] E. L. Ivchenko and G. E. Pikus, *Superlattices and Other Heterostructures* (Springer, Berlin, 1997).
[2] A. V. Kavokin, V. P. Kochereshko, G. R. Posina, I. N. Uraltsev, D. R. Yakovlev, G. Landwehr, R. N. Bicknell-Tassius, and A. Waag, Phys. Rev. B **46**, 9788 (1992).
[3] L. A. Kolodziejski, R. L. Gunshor, N. Otsuk, S. Datta, W. M. Becker, and A. V. Nurmikko, IEEE J. Quantum Electron. **32**, 1666 (1986).
[4] K. Shahzad, D. J. Olego, and C. G. Van de Walle, Phys. Rev. B **38**, 1417 (1988).
[5] H. J. Lozykowski and V. K. Shastri, J. Appl. Phys. **69**, 3235 (1991).
[6] U. Streller, N. Hoffmann, A. Schulzgen, J. Griesche, H. Babucke, F. Henneberger, and K. Jakobs, Semicond. Sci. Technol. **10**, 201 (1995).
[7] J. Puls, M. Rabe, A. Siarkos, and F. Henneberger, Phys. Rev. B **57**, 14749 (1998).
[8] G. V. Astakhov *et al.*, Phys. Rev. B **65**, 165335 (2002).
[9] H. Mariette, F. Dal'bo, N. Magnea, G. Lentz, and H. Tuffigo, Phys. Rev. B **38**, 12443 (1988).
[10] M. Cardona, *Modulation Spectroscopy* (Academic, New York, 1969).
[11] M. Cardona, Phys. Status Solidi B **198**, 5 (1996).
[12] A. K. Dutta and K. Kasahara, Solid State Electronics **42**, 907 (1998).
[13] Y. K. Kato, R. C. Myers, A. C. Gossard, and D. D. Awschalom, Phys. Rev. Lett. **93**, 176601 (2004).
[14] G. E. Pikus and G. L. Bir, Sov. Phys. Solid State **1**, 1502 (1959).
[15] T.-Y. Chung, J. H. Oh, S. G. Lee, J.-W. Jeong, and K. J. Chang, Semicond. Sci. Tech. **12**, 701 (1997).
[16] H. W. Hölscher, A. Nöthe, and C. Uihlein, Phys. Rev. B **31**, 2379 (1985).
[17] K. L. Teo, Y. P. Feng, M. F. Li, T. C. Chong, and J. B. Xia, Semicond. Sci. Tech. **9**, 349 (1994).
[18] D. Rached, N. Benkhettou, B. Soudini, B. Abbar, N. Sekkal, and M. Driz, Phys. Status Solidi B **240**, 565 (2003).
[19] C. Thomsen, H. T. Grahn, H. J. Maris, and J. Tauc, Phys. Rev. B **34**, 4129 (1986).
[20] A. V. Akimov, A. V. Scherbakov, D. R. Yakovlev, C. T. Foxon, and M. Bayer, Phys. Rev. Lett. **97**, 037401 (2006).
[21] A. V. Scherbakov, P. J. S. van Capel, A. V. Akimov, J. I. Dijkhuis, D. R. Yakovlev, T. Berstermann, and M. Bayer, Phys. Rev. Lett. **99**, 057402 (2007).
[22] T. Berstermann, C. Brüggemann, M. Bombeck, A. V. Akimov, D. R. Yakovlev, C. Kruse, D. Hommel, and M. Bayer, Phys. Rev. B **81**, 085316 (2010).
[23] Landolt-Börnstein, *II-VI and I-VI Compunds: Semimagnetic Compounds*, edited by U. Rössler (Springer, Berlin, 1999).
[24] D. R. Yakovlev, G. V. Astakhov, W. Ossau, S. A. Crooker, K. Uchida, N. Miura, A. Waag, N. A. Gippius, A. Y. Sivachenko, and A. B. Dzyubenko, Phys. Status Solidi B **227**, 353 (2001).
[25] A. A. Sirenko, T. Ruf, M. Cardona, D. R. Yakovlev, W. Ossau, A. Waag, and G. Landwehr, Phys. Rev. B **56**, 2114 (1997).
[26] D. Wolverson, J. J. Davies, C. L. Orange, K. Ogata, S. Fujita, K. Nakano, H. Okuyama, S. Itoh, B. Jobst, and D. Hommel, Phys. Rev. B **60**, 13555 (1999).
[27] J. J. Davies *et al.*, Phys. Rev. Lett. **97**, 187403 (2006).
[28] L. C. Smith *et al.*, Phys. Rev. B **78**, 085204 (2008).
[29] J. J. Davies, L. C. Smith, D. Wolverson, A. Gust, C. Kruse, D. Hommel, and V. P. Kochereshko, Phys. Rev. B **81**, 085208 (2010).
[30] N. A. Gippius, A. L. Yablonskii, A. B. Dzyubenko, S. G. Tikhodeev, L. V. Kulik, V. D. Kilakovskii, and A. Forchel, J. Appl. Phys. **83**, 5410 (1998).